

Supernova scores for active anomaly detection

T. A. Semenikhin^{a,b,*}, M. V. Kornilov^{a,c}, M. V. Pruzhinskaya^a, V. V. Krushinsky^d, K. L. Malanchev^e, A. V. Dodin^a

^a*Lomonosov Moscow State University, Sternberg astronomical institute, Universitetsky pr. 13, Moscow, 119234, Russia*

^b*Lomonosov Moscow State University, Faculty of Physics, Leninskie Gory 1-2, Moscow, 119991, Russia*

^c*National Research University Higher School of Economics, 21/4 Staraya Basmannaya Ulitsa, Moscow, 105066, Russia*

^d*Laboratory of Astrochemical Research, Ural Federal University, Ekaterinburg, ul. Mira d. 19, Yekaterinburg, 620002, Russia*

^e*McWilliams Center for Cosmology and Astrophysics, Department of Physics, Carnegie Mellon University, Pittsburgh, PA 15213, USA*

Abstract

Large time-domain sky surveys generate extensive multi-year catalogs of light curves in which scientifically valuable transients, such as supernovae (SNe), are vastly outnumbered by artifacts and routine star variability. While supervised machine learning models can efficiently filter known classes, they struggle with extreme class imbalance and may overlook rare or novel events. Conversely, unsupervised anomaly detection provides broad discovery potential but lacks targeted sensitivity. We present a hybrid strategy that integrates a supervised SN probability score (SN-score) into the PineForest active anomaly detection framework to enhance SN discovery rate in the 23rd data release of the Zwicky Transient Facility. We train a binary classifier using light-curve features of spectroscopically confirmed SNe from the ZTF Bright Transient Survey, achieving a $\text{ROC} \sim \text{AUC} \approx 0.98$. Incorporating the SN-score as an additional feature, together with a small set of labeled priors, significantly accelerates the discovery of SN-like transients across ten extragalactic ZTF fields. This method increases discovery efficiency without compromising the ability to identify diverse astrophysical anomalies. Application of the combined methodology resulted in the discovery of seven previously unreported SN candidates, one AGN candidate, one unusual Galactic variable star SNAD283, as well as two host galaxies exhibiting multiple supernova events. These results demonstrate its value for scalable and expert-guided transient search in current and future surveys, including the Vera C. Rubin Observatory Legacy Survey of Space and Time.

Keywords: Astronomy data analysis, Classification, Outlier detection, Sky surveys, Supernovae

1. Introduction

Time-domain astronomy has entered an era of unprecedented data volume. Modern large-scale sky surveys, such as the Zwicky Transient Facility (ZTF, Bellm et al. 2019) and the forthcoming Vera C. Rubin Observatory Legacy Survey of Space and Time (LSST, LSST Science Collaboration et al. 2009), generate up to hundreds of thousands to millions of alerts per night, revealing diverse classes of variable and transient astrophysical phenomena. At these scales, identifying rare and scientifically valuable transients becomes extremely challenging. Many detections correspond to instrumental artifacts, spurious signals induced by atmospheric or observational conditions, or objects of non-astrophysical nature (Masci et al., 2019; Mahabal et al., 2019; Malanchev et al., 2021; Karpov and Peloton, 2023). Even among real signals, only a small subset may be relevant for a specific scientific objective, while the rest constitute background variability of little interest to a given research program. This imbalance between data volume and scientific relevance motivates the development of efficient automatic methods capable of distinguishing rare, high-value transient events from the overwhelming population of routine detections.

Traditional transient-classification pipelines rely on supervised machine-learning models trained on labelled datasets (Richards et al., 2011; Bloom et al., 2012; Wright et al., 2015). While such models have achieved high performance in filtering astrophysical events from artifacts (Aldering et al., 2002; Bailey et al., 2007; Duev et al., 2019) and discriminating between transient types, they inherently struggle with class imbalance and cannot naturally adapt to new or rare phenomena. At the same time, purely unsupervised anomaly detection methods have emerged as powerful tools for discovering unexpected events in large unlabeled datasets (Pruzhinskaya et al., 2019; Webb et al., 2020; Malanchev et al., 2021; Villar et al., 2021). However, these approaches often lack sensitivity to specific object classes of interest unless explicitly guided (Majumder et al., 2024; Pruzhinskaya, M. V. et al., 2023).

Active anomaly detection frameworks combine the strengths of unsupervised learning with expert feedback, enabling iterative exploration of rare events in vast astronomical datasets (e.g. Ishida, E. E. O. et al. 2021; Kornilov et al. 2025; Gómez et al. 2025). By integrating domain knowledge in the form of human labels or prior examples, these methods provide a flexible and scalable strategy for targeted discovery while retaining the ability to detect other astrophysical outliers. In practice, a key challenge lies in incorporating available information about known rare classes — such as SNe — without

*Corresponding author.

Email address: semenikhintimofey@gmail.com (T. A. Semenikhin)

compromising the algorithm’s potential to uncover genuinely unexpected objects.

In this work, we introduce the hybrid methodology to perform a supernova (SN) search. We develop a supervised binary classifier trained to distinguish SNe from non-SNe using a list of SNe from the Zwicky Transient Facility Bright Transient Survey (ZTF BTS, Perley et al. 2020) cross-matched with ZTF Data Release 23 (DR23). The resulting SN probability score (SN-score), computed for nearly four million objects across ten extragalactic fields in ZTF DR23, is then employed as an additional informative feature within the PineForest active anomaly detection framework (Ishida et al., in prep.). The purpose of this hybrid strategy is two-fold: (1) to enable the anomaly detection algorithm to autonomously determine a SN detection threshold for particular feature subspace, and (2) to accelerate the identification of transient events with SN-like photometric behavior, without precluding the discovery of other astrophysically interesting anomalies.

The article is organized as follows. In Section 2, we describe the datasets used in this work. Section 3 outlines the preprocessing pipeline. In Section 4, we introduce the binary SN classifier. Section 5 presents the active anomaly detection framework and examines the impact of incorporating the proposed SN-score. The main findings are described in Section 6. Conclusions are given in Section 7. Finally, the Appendix 7 provides the full list of features and discusses the feature importance.

2. Data

2.1. Zwicky Transient Facility

In this work we used data from the Zwicky Transient Facility¹ wide-field sky survey. ZTF is conducted at the Palomar Observatory in California, USA, using a 1.26-m Samuel Oschin telescope with a field of view of approximately 47 square degrees. The survey operates in three photometric passbands (z_g , z_r , z_i , Bellm et al. 2019). Data from ZTF are provided in two formats: alerts and data releases. Alerts are issued in real-time, while data releases contain light curves of variable objects over the entire observation period. In this work, we use the z_r -band light curves from the DR23 for classification and anomaly detection part; light curves in all available passbands for further analysis of SN candidates. ZTF DR23 contains approximately 4.97 billion light curves. By applying the following selection criteria to all z_r -band light curves from ZTF DR23: $58178 \leq \text{MJD} \leq 60125$ and number of good observations per light curve ≥ 100 (this condition leads to the fact that we consider the light curves of only the ZTF primary tiling grid, see Section 2.9 in Bellm et al. 2018), we obtained a *main* dataset comprising about 720 million light curves.

It is important to emphasize that we did not perform any cross-matching between the light curves in a whole main dataset. Consequently, multiple light curves in this dataset may correspond to the same astrophysical source on the sky. We

discuss the causes of this in more detail in Section 3.2, but here we note that within the framework of the main dataset this is not critical for us, since we do not train any models sensitive to such duplicates on it entirely.

In the ZTF DRs, the entire northern sky is divided into fields identified by specific `Field` ID numbers. The top part in Fig. 1 presents a heatmap showing the distribution of object counts across these fields for our main dataset. Since the main dataset contains an extremely large number of objects, it is not feasible to perform active anomaly detection experiments on the full set. Therefore, we limited our analysis to a subset of 10 fields.

The selection of these fields was guided by several criteria: (1) the fields are located outside the Galactic plane ($|b| > 20$ deg); (2) the fields overlap with other survey projects (see the bottom part in Fig. 1); and (3) several fields are elongated along the same Galactic longitude in order to account for population changes of Galactic anomalies with Galactic latitude. Considering these factors, we selected the fields indicated by blue rectangles in Fig. 1 for the active anomaly detection experiments.

2.2. Bright Transient Survey

To construct a classifier distinguishing SNe from non-SNe, we require a sample of confirmed SNe with corresponding observations available in ZTF DR23. For this purpose, we used data from the ZTF BTS.

The ZTF BTS is a large spectroscopic SN survey that has operated since 2018, targeting nearly all extragalactic, non-AGN transients brighter than 18.5–19 mag across the northern sky. As of 2025, it includes over 11,000 spectroscopically confirmed transients, the vast majority of which are SNe. BTS achieves a spectroscopic completeness of approximately 95% for well-sampled, SN-like light curves, with most of the remaining incompleteness due to weather or operational gaps. The survey applies well-defined selection criteria to construct a high-quality statistical sample and provides subtype information when available. Although the main survey phase has ended, BTS continues to classify all bright transients and those in nearby galaxies down to fainter limits, ensuring a nearly complete and uniform sample of bright SNe from ZTF.

We selected all classified SNe from the BTS, then retained only those that satisfy the BTS quality criteria, and further restricted the sample to objects whose peak end date fall within $58178 \leq \text{MJD} \leq 60125$. As a result, out of approximately 11,000 SNe in BTS, the sample of 4,832 objects remained.

3. Preprocessing

3.1. Feature extraction

In machine learning, before applying a specific algorithm to the data, it is often necessary to perform an intermediate step – feature extraction. In our case, this step is essential, since the light curves provided in the ZTF DRs are irregularly sampled in time and vary in length. To convert the data into a tabular format suitable for analysis, we used the Python library

¹<https://www.ztf.caltech.edu/>

light-curve² (Malanchev et al., 2021), which enables the extraction of informative astronomical features from light curves.

The set of 47 extracted features is hereafter referred to as the *initial* feature set. The complete list of these features is provided in Appendix A. We extracted features for all light curves in the main dataset using 14 cores of a dual Intel Xeon Gold 5118 system, which took approximately 235 hours. The resulting file contains about 720 million rows and has a total size of 127 GB.

3.2. Cross-matching

The BTS sample provides sky coordinates for each object, which allowed us to cross-match these SNe with objects from our main dataset. This was done using an application programming interface³ that, given celestial coordinates and a search radius, returns all object IDs (OIDs) from ZTF DR23 located within the specified area. Using this tool, we retrieved all objects from the main sample lying within a 2-arcsecond radius centered on each BTS supernova. In cases where multiple matches were found within this radius, we selected the object with the largest number of observations in the *zr* filter. This choice is motivated by the fact that, in ZTF, a single astrophysical source may be assigned different OIDs when it falls near the boundary between two fields, resulting in its light curve being split across multiple OIDs. Since these OIDs correspond to the same physical source, we adopt the OID with the greatest number of *zr*-band observations, assuming it provides the most complete and temporally well-sampled representation of the underlying light curve. As a result of this cross-matching procedure, we obtained a list of 2,066 objects from our main sample those overlap with BTS sample. After visual inspection of all candidates, the final sample contained 674 SNe.

4. Binary SN classifier

We employed a standard supervised classification approach, in which each object is represented by a set of initial features. During training, these features are provided to the model along with class labels, allowing it to learn a mapping between feature space and object type. During inference, the model receives only the feature vectors of unlabeled objects and outputs a continuous SN-score that can be interpreted as the probability of the object being a SN according to the classifier.

4.1. Train dataset

Since the fraction of SNe in the main dataset is extremely small, it was not feasible to develop the classifier using a balanced training sample (see Appendix B). For training, we assigned positive class to all 674 confirmed SNe (see Section 2.2), while the negative class included 6300 non-SN objects from the Anomaly Knowledge Base (AKB; see Section 4 in Malanchev et al. 2023) together with 10,000 randomly selected objects from the main dataset. This approach makes the classifier more conservative, reducing the frequency of high SN-scores and thereby improving its overall precision.

4.2. Model

For the binary classifier, we chose a Random Forest (Breiman, 2001) model, as previous studies (Semenikhin et al., 2025) have shown that popular machine learning methods achieve comparable performance on similar tasks. As described in Section 4.1, we used an unbalanced SN sample and additionally assigned class weights of 1:1000 in the Random Forest to prevent the model from ignoring the rare class. Otherwise, we used the default parameters from the `scikit-learn`⁴ implementation (number of trees – 100, the minimum number of samples required to split an internal node – 2, criterion – Gini).

To evaluate the performance of the final binary classifier, we used stratified k-fold ($k = 5$) cross-validation, which accounts for class imbalance when splitting the data into folds. The primary performance metric was the ROC-AUC, which is threshold-independent; the final classifier achieved a ROC – AUC = 0.98 ± 0.011 (see Fig. 2).

5. Anomaly detection

The concept of anomaly detection is to identify unusual astrophysical objects within an unlabeled dataset. In our case, we search for such objects within a small subset of the main dataset – specifically, in the 10 selected fields (see Section 2.1). In general, anomaly detection operates by taking objects represented in some feature space (in our case, light-curve features) and feeding them into a model that estimates the density distribution of objects within this space, ranking them from the most to the least common. The main innovation proposed in this work is to incorporate the predictions of a binary SN classifier as an additional feature in the initial feature set, resulting in an *augmented* feature set. This approach allows the anomaly detection method to determine the optimal decision threshold of the classifier autonomously.

Traditional static anomaly detection methods, such as Isolation Forest (Liu et al., 2008), do not account for the specific preferences of an expert and do not incorporate user feedback. In contrast, active anomaly detection methods allow the model to adapt dynamically to expert input during the exploration process. In this work, we tested the performance of `PineForest`, an implementation available in the Python library `Coniferest` (Kornilov et al., 2025).

5.1. PineForest

This is an iterative algorithm whose first step is the initialization of an Isolation Forest. The expert is then presented with the most anomalous object in the dataset, which is carefully examined using all available information sources. The expert labels the object as **A** (anomalous, i.e., scientifically interesting), **R** (regular, a typical object of no particular interest), or **U** (unknown, when a confident judgment cannot be made; such objects are excluded from the dataset and do not affect model

²<https://github.com/light-curve/light-curve-python>

³<https://db.ztf.snad.space/api/v3/help>

⁴<https://scikit-learn.org/stable/>

training). Next, PineForest randomly constructs additional trees and evaluates their performance together with the existing ones in the model, assessing which trees best align with the expert’s feedback and discarding a fraction of those that perform poorly. The remaining trees are retained in the model, and the process repeats iteratively until a predefined review budget is reached.

Despite the adaptive nature of this algorithm, achieving high-quality model performance may sometimes require a large review budget. However, if the expert has prior knowledge of the object type to be discovered and possesses examples of confirmed, classified instances within the dataset, PineForest allows these to be provided as priors. In this case, immediately after the initialization step of the Isolation Forest, PineForest prunes trees that are inconsistent with the supplied priors. The algorithm then proceeds following the standard iterative procedure. Initial experiments have demonstrated that providing even a small number of priors (as few as ten) can significantly accelerate the anomaly detection process (see Table 1).

5.2. Evaluation

To evaluate the performance of the proposed approach, we measured how many SNe were recovered by PineForest among the 30 visually inspected candidates in different experiments. We conducted experiments both without and with priors, using the initial and the augmented feature sets. Table 1 summarizes the results for each field, showing the number of SNe identified among the 30 examined candidates. The last column of the table reports the number of SNe found within the top 30 objects ranked by the binary classifier’s SN-score.

To assess the statistical significance of the observed differences between the experimental setups, we complemented the main results (Table 1) with a comparative analysis using Fisher’s exact test (Table 2). Fisher’s exact test evaluates whether two categorical variables are independent by calculating the probability of obtaining the observed contingency table under the null hypothesis. In our case, the null hypothesis (H_0) states that both methods under comparison recover SNe with equal efficiency, while the alternative hypothesis (H_1) assumes that the second method yields a higher detection rate. The resulting p-value quantifies the probability of obtaining the observed (or more extreme) results under H_0 ; values below 0.05 are typically considered statistically significant.

For each pair of methods, the contingency tables summarize the number of detected and non-detected SNe across the ten ZTF fields. The Odds Ratio indicates the relative likelihood of successful detection by the first method compared to the second: values below 1 imply that the second method performs better, while values above 1 favor the first method.

The results (Table 2) show that introducing priors in combination with the augmented feature set leads to a highly significant improvement ($p \ll 0.05$), confirming the benefit of guiding the anomaly detection algorithm with even a small number of known examples. In contrast, adding priors to the initial feature set or using the augmented features alone without priors did not produce statistically significant gains. Interestingly, the comparison between the augmented feature set with priors and

the simple ranking by the binary classifier’s SN-score reveals no significant difference ($p = 0.50$), indicating that both approaches yield comparable SN recovery rates across the tested fields. This is further supported by a strong Spearman rank correlation ($\rho = 0.82$) between their field-wise detection counts, indicating consistent detection behavior. Although these results may appear to lessen the role of active anomaly detection in the specific task of SN recovery, it is important to stress that our broader objective is not to perform a binary SN/non-SN classification (such events are already efficiently identified within the alert stream). Instead, these experiments serve to demonstrate that our approach can effectively highlight the regions of feature space most relevant to the phenomena of interest, while simultaneously making this space more structured and discriminative through the inclusion of an additional informative feature. In future applications, our goal is to target much rarer transients, such as gravitational lenses, and we expect that the proposed approach will help guide the search toward these scientifically valuable outliers.

6. Discovered transients and special cases in ZTF DR23

During the development of the binary classifier and the subsequent PineForest experiments, seven previously unreported SN candidates, one AGN candidate and one unusual variable star were identified in ZTF DR23. Although all of these events appeared in the ZTF alert stream (as indicated by their assigned ZTF IDs), but they were not flagged as noteworthy by broker pipelines and therefore escaped earlier attention. All discovered objects have been submitted to the Transient Name Server⁵ (TNS), and they are listed in Table 3. The first column contains the internal SNAD object name; the second – the corresponding ZTF identifier; the third – unique ZTF DR OID; the equatorial coordinates in degrees are given in column 4; the peak absolute magnitude in the zr band, $M_{r,\max}$, derived from the best-fitting light-curve model is shown in column 5; and the preferred classification is given in column 6.

6.1. Supernova candidates

We performed an initial light curve analysis of seven SN candidates using the Python package SNCOSMO⁶. For each candidate, the light curves in all available passbands (z , r , i) were fitted with the Nugent’s SN models⁷ and the SALT2 model (Betoule et al., 2014). The Nugent’s templates are simple spectral time-series parameterized by redshift (z), the observer-frame time corresponding to the explosion moment (t_0) and the amplitude.

The SALT2 model, developed for Type Ia SNe, describes the spectral energy distribution as a combination of a mean template, a variability component governing light curve shape, and a color law. Its free parameters are stretch parameter (x_1), color parameter (c), redshift, amplitude and time of maximum light.

⁵<https://www.wis-tns.org/>

⁶<https://sncosmo.readthedocs.io/en/stable/>

⁷https://c3.lbl.gov/nugent/nugent_templates.html

Field ID	initial		augmented		top30 SN-score
	without priors	with priors	without priors	with priors	
252	1	0	1	1	0
401	1	2	1	4	3
468	0	0	0	0	1
795	0	2	0	8	8
848	0	4	0	9	6
797	0	0	0	8	8
759	0	0	0	1	3
718	2	5	2	8	8
673	1	0	0	4	6
626	2	1	0	2	1

Table 1: Results of the PineForest runs on the selected fields (see Section 2.1). The table lists the numbers of SNe identified among top 30 visually inspected candidates. Before performing the anomaly search, all SNe used in the classifier training were removed from the fields. The best result for each field is highlighted in bold.

To mitigate host–galaxy contamination in the ZTF photometry, we subtracted the reference magnitudes provided in the SNAD catalogue⁸. The light curves were further corrected for Galactic extinction using the line-of-sight reddening estimates of Schlafly and Finkbeiner (2011). For each SNAD SN candidate, the preferred model was selected by minimizing the χ^2 statistic. The light curve fitting results for the discovered SNe are shown in Fig. 3 and 6, and the optimized model parameters are listed in the corresponding panels. Based on the best-fitting photometric models, our sample consists of five SNe Ia, one SN IIn, and one SN IIP.

6.2. A Galactic helium-rich transient: SNAD283

SNAD283 was initially identified as a potential superluminous supernova candidate, based on a single SN-like outburst with a broad light curve lasting for more than one year. To determine its redshift and nature, we obtained a spectrum (Fig. 4) with the Transient Double-beam Spectrograph (TDS) mounted on the 2.5-m telescope of the Caucasus Mountain Observatory (CMO; Potanin et al. 2020; Shatsky et al. 2020).

The spectrum shows that the source is a Galactic object. It is dominated by strong helium double-peaked emission lines, indicating a helium-rich accretion disc. While the event duration is compatible with that of some classical novae, its outburst amplitude is small (about 3 mag), which is significantly lower than typically observed for novae. In contrast, although the amplitude is compatible with dwarf novae, the duration of the event is significantly longer than usually observed for this class (Fig. 5). Further observations and analysis are therefore required to clarify the origin of this event.

6.3. Multiple supernovae

Multiple supernovae refer to cases in which two or more supernovae explode in the same host galaxy (so-called supernova siblings). Such systems are useful tool to investigate possible connections between SN spectroscopic types and their

host–galaxy environments (Salo et al., 2025). In addition, supernova siblings can be used to assess systematic effects in distance measurements, which is important for cosmological applications (Gall et al., 2018). More generally, they offer a way to probe the properties of the progenitor stellar populations and the host galaxies, including star-formation rate, dust extinction, and metallicity (e.g. Graham et al. 2022).

In practice, studies of supernova siblings usually focus on cases where multiple transients in the same host galaxy are clearly spatially separated, so that they can be unambiguously identified as independent sources. However, at larger distances the apparent angular size of galaxies decreases, and multiple explosions occurring within a single host may appear unresolved for the particular survey. In such cases, it becomes non-trivial to determine whether we are observing two independent supernovae in the same galaxy, or multiple outbursts from a single source. The latter scenario includes so-called supernova impostors, which are believed to be non-terminal eruptions, often associated with luminous blue variables, such as η Carinae. Although these events are also of great astrophysical interest, their physical mechanisms are still not well understood (Smith et al., 2011).

During the development of the binary classifier and the subsequent anomaly-detection experiments, we identified two galaxies hosting pairs of supernova siblings that, to our knowledge, have not been previously reported in the literature⁹. Below, we present an initial analysis of the relative positions of these transients within their host galaxies, followed by individual light-curve modelling for each event, performed in the same manner as for the new SN candidates described in Section 6.1.

6.3.1. AT2018mpv/SNAD287 and AT2023kuz/ATLAS23mmv

The light curve shows two outbursts separated by more than five years (see Fig. 6). The first outburst appeared in the

⁸<https://snad.space/catalog/>

⁹We also encountered two additional similar cases in other SNAD-related studies: a re-brightening of the superluminous SN 2018feg about 3.5 years after the main outburst (Majumder et al., 2024), and two transients, SN 2019rra and AT 2020aewi, occurring in the same host galaxy (Gangler et al., in prep.).

Comparison	Contingency table (SNe / non-SNe)	Odds Ratio	p-value	Interpretation
initial without priors vs. initial with priors	$\begin{bmatrix} 7 & 293 \\ 14 & 286 \end{bmatrix}$	0.49	0.09	Moderate difference, not statistically significant ($p > 0.05$). Using priors without SN-scores likely improves the result, but evidence is insufficient.
augmented without priors vs. augmented with priors	$\begin{bmatrix} 4 & 296 \\ 45 & 255 \end{bmatrix}$	0.08	10^{-11}	Highly significant difference — adding priors to augmented feature set substantially improves performance ($p \ll 0.05$).
initial without priors vs. augmented without priors	$\begin{bmatrix} 7 & 293 \\ 4 & 296 \end{bmatrix}$	1.77	0.90	No significant difference between the initial and augmented feature set when priors are not used.
initial with priors vs. augmented with priors	$\begin{bmatrix} 14 & 286 \\ 45 & 255 \end{bmatrix}$	0.28	10^{-5}	Adding SN-scores to features significantly improves the results, when we use priors.
top30 SN-score vs. augmented with priors	$\begin{bmatrix} 44 & 256 \\ 45 & 255 \end{bmatrix}$	0.97	0.50	No significant difference; both methods show very similar behavior across fields.

Table 2: Results of pairwise Fisher’s exact tests between different detection methods. The contingency tables show the number of detected versus non-detected SNe for each pair of methods. The reported one-sided p-values correspond to Fisher’s exact tests under the hypothesis that the second method performs better than the first.

ZTF alert stream as ZTF19aaltuxk, but was not reported to TNS at the time of the event. We later reported it to TNS as AT2018mpv on 2025-07-30 (Semenikhin, 2025). The second outburst was reported to TNS as AT2023kuz by the ATLAS survey (Tonry et al., 2023).

To measure the offset between the second outburst and the host-galaxy nucleus relative to the first outburst, we used stacked zr -band images obtained by ZTF between 2018-05-05 and 2018-07-07 for the first outburst, and between 2023-06-13 and 2023-06-27 for the second outburst. The position of the host galaxy was determined from stacked images obtained between 2022-02-12 and 2022-05-28. Source positions were measured using two-dimensional Gaussian fitting. The measured offset between the two outbursts does not exceed the 1σ positional uncertainty (see Fig. 7); therefore, we cannot conclude that the two outbursts originate from independent sources.

In order to classify the transients and to determine the redshift of the host galaxy, we obtained a spectrum of the host on 2026 January 29 at 02:52:42 UTC with TDS of the 2.5-m CMO telescope (Shatsky et al., 2020). The positions of the emission lines yield a redshift of $z = 0.09942 \pm 0.00002$ ¹⁰.

Using this redshift, we modelled the outbursts with SNCOSMO. The fitting results are shown in the bottom panels of Fig. 6. For both outbursts, a Type Ia supernova classification is the most plausible.

6.3.2. SN2018elp and AT2022mwi

The light curve shows two outbursts separated by approximately four years. These transients were previously reported to TNS as SN2018elp (Tonry et al., 2018) and AT2022mwi.

We measured the positional offsets of both outbursts with respect to the host galaxy (Fig. 8). The position of the first outburst was measured from stacked images obtained between 2018-08-01 and 2018-08-18, and that of the second outburst from stacked images obtained between 2022-06-10 and 2022-06-28. The difference between the two measured positions exceeds 16σ , indicating that these events are spatially distinct. We therefore conclude that they are supernova siblings.

The first outburst, SN2018elp, is classified in TNS as a Type II supernova with a measured redshift of $z = 0.03$ (Stein et al., 2018). We adopted this redshift for the SNCOSMO modelling of both transients. The photometric classification of SN2018elp as SN IIP is consistent with its spectroscopic classification. For AT2022mwi the best-fitting model corresponds to a Type Ibc supernova (see Fig. 9).

7. Conclusions

In this work, we introduced a SN-score designed to enhance active anomaly detection in wide-field time-domain astronomical surveys. Using light curves from ZTF DR23 and spectroscopically confirmed events from the BTS, we constructed a binary classifier capable of distinguishing SNe from non-SN sources. The classifier achieves high performance (ROC-AUC

¹⁰<https://www.wis-tns.org/object/2018mpv>

Name	ZTF ID	OIDs	α, δ (deg)	$M_{r,max}$	Classification
SNAD280	ZTF20aanskdl	790209200005857	195.95520 55.91314	-18.62^m	Ia
SNAD281	ZTF19aarisy1	676207400000993	219.21985 32.27425	-19.95^m	IIn
SNAD282	ZTF18aarqjgu	676212300024137	215.84439 33.72295	-16.36^m	Ia
SNAD283	ZTF23aaaptpf	787210100006486	161.37753 56.05923	–	VS of MW galaxy
SNAD284	ZTF19aawvklc	759201400013865	229.08777 44.56771	-18.87^m	Ia
SNAD285	ZTF18abmkbqk	759209300030421	227.80917 48.55150	-15.67^m	Ia
SNAD286	ZTF21acmivtg	252216200002097	49.73880 -20.91431	-19.50^m	IIP
SNAD287	ZTF19aaltuxk	533202300011210	243.77243 8.83445	-19.11^m	Ia
SNAD288	ZTF22abeuuvu	650202200001826	17.11930 31.16565	–	AGN

Table 3: Transients identified during the anomaly detection experiments. The values of $M_{r,max}$ and classification of SN candidates inferred from the SNCOSMO light-curve fits.

≈ 0.98) and provides a quantitative score that can be incorporated as an additional feature for anomaly detection algorithms.

We integrated this score into the PineForest – an active anomaly detection framework, and demonstrated that it substantially improves the recovery of SNe when combined with a small number of labeled priors. Our experiments across ten extragalactic ZTF fields show that the augmented feature set enables the algorithm to converge more rapidly toward scientifically relevant candidates, increasing the efficiency of expert-guided exploration of large unlabeled datasets. Importantly, the approach retains the ability to detect diverse astrophysical anomalies rather than simply replicating supervised classification.

Application of the combined methodology resulted in the discovery of seven previously unreported supernova candidates, one AGN candidate, and one unusual Galactic variable star. Photometric modelling of the seven supernova candidates with SNCOSMO indicates a sample composed of five SNe Ia, one SN IIn, and one SN IIP. Spectroscopic follow-up of the peculiar source SNAD283 suggests a Galactic helium-rich accreting system, whose long-lasting and low-amplitude outburst is inconsistent with classical nova or dwarf-nova behaviour. We also report two host galaxies exhibiting multiple supernova events and present their astrometric and photometric analyses. These results demonstrate the ability of the hybrid approach to efficiently discover supernovae and other rare or ambiguous transients in large-scale surveys.

The methods developed here are applicable to ongoing and future time-domain experiments, including the Vera C. Rubin Observatory LSST¹¹, which will require scalable, adaptive, and expert-steerable systems for identifying and prioritising scientifically interesting objects.

Acknowledgements

T. Semenikhin, M. Kornilov and M. Pruzhinskaya acknowledge support from a Russian Science Foundation grant 24-22-

00233, <https://rscf.ru/en/project/24-22-00233/> for conceptualization, software development of the proposed algorithm; conducting experiments and analyzing of obtained results. T. Semenikhin acknowledges support from the Theoretical Physics and Mathematics Advancement Foundation “BASIS” for formalizing the proposed approach in a repository on GitHub and publishing the data on Zenodo. Support was provided by Schmidt Sciences, LLC. for K. Malanchev. The work was carried out using equipment developed with the support of the M.V. Lomonosov Moscow State University Program of Development.

Appendix A. List of features

Table A.4 lists all features used in this work along with their brief descriptions. A more detailed explanation of each feature can be found in the `light-curve-feature` Rust crate documentation¹².

Appendix B. Feature importance and class balance

At the initial stage, we trained the binary classifier on a balanced dataset. In this configuration, the sample was relatively small (about 1500 objects), and the resulting performance metrics, including the ROC-AUC, appeared high. However, inspection of the feature-importance diagram revealed that the most influential features were the reduced χ^2 values associated with linear and Bazin function fits, while all other features contributed negligibly. This effect arises because brighter objects have smaller measurement uncertainties. Since the χ^2 statistic is inversely weighted by the observational errors, even small residuals can produce relatively large χ^2 values, despite the model light curve visually providing a good fit to the data points. As a result, the classifier implicitly learned to label faint sources as non-SNe. Since most BTS SNe in our training set

¹¹<https://www.lsst.org/>

¹²https://docs.rs/light-curve-feature/latest/light_curve_feature/features/index.html

Extractor	Number of features	Remark
Extracted from magnitude		
Amplitude	1	
Mean	1	
Kurtosis	1	
Median Absolute Deviation	1	
Anderson Darling Normal	1	Unbiased Anderson–Darling normality test statistic
Cusum	1	A range of cumulative sums
BeyondNStd	1×2	Fraction of observations beyond $N\sigma_m$ (for $N = 1, 2$) from the mean magnitude
Inter Percentile Range	1×3	Inter-percentile range $Q(1 - p) - Q(p)$, where $Q(p)$ is the p th quantile of the magnitude distribution (for $p = 0.02, 0.1, 0.25$)
Linear Fit	3	Slope, its error and reduced χ^2 of the light curve in the linear fit
Linear Trend	3	The slope, its error and noise level of the light curve in the linear fit
Periodogram	$2 \times \text{peaks} + 4$	Peaks of Lomb–Scargle periodogram and periodogram as a meta-feature (for peaks = 5)
Reduced χ^2	1	
Skew	1	Skewness of magnitude $G1$
Standard Deviation	1	
StetsonK	1	Stetson K coefficient described light curve shape
Weighted Mean	1	
Extracted from flux		
Otsu Split	4	
Mean Variance	1	Standard deviation to mean ratio
Bazin Fit	5	
Excess Variance	1	Measure of the variability amplitude
Total number of features:	47	

Table A.4: Feature set used in this study.

are relatively bright, this bias inflated the performance metrics, but led to numerous false positives during inference (most notably bright artifacts). To mitigate this issue, we adopted the sampling strategy described in Section 4.

References

- Aldering, G., Adam, G., Antilogus, P., Astier, P., Bacon, R., Bongard, S., Bonnaud, C., Copin, Y., Hardin, D., Henault, F., Howell, D.A., Lemonnier, J.P., Levy, J.M., Loken, S.C., Nugent, P.E., Pain, R., Pecontal, A., Pecontal, E., Perlmutter, S., Quimby, R.M., Schahmaneche, K., Smadja, G., Wood-Vasey, W.M., 2002. Overview of the Nearby Supernova Factory, in: Tyson, J.A., Wolff, S. (Eds.), *Survey and Other Telescope Technologies and Discoveries*, pp. 61–72. doi:10.1117/12.458107.
- Bailey, S., Aragon, C., Romano, R., Thomas, R.C., Weaver, B.A., Wong, D., 2007. How to Find More Supernovae with Less Work: Object Classification Techniques for Difference Imaging. *ApJ* 665, 1246–1253. doi:10.1086/519832, arXiv:0705.0493.
- Bellm, E.C., Kulkarni, S.R., Graham, M.J., Dekany, R., Smith, R.M., Riddle, R., Masci, F.J., Helou, G., Prince, T.A., Adams, S.M., Barbarino, C., Barlow, T., Bauer, J., Beck, R., Belicki, J., Biswas, R., Blagorodnova, N., Bodewits, D., Bolin, B., Brinnet, V., Brooke, T., Bue, B., Bulla, M., Burruss, R., Cenko, S.B., Chang, C.K., Connolly, A., Coughlin, M., Cromer, J., Cunningham, V., De, K., Delacroix, A., Desai, V., Duev, D.A., Eadie, G., Farnham, T.L., Feeney, M., Feindt, U., Flynn, D., Franckowiak, A., Frederick, S., Fremling, C., Gal-Yam, A., Gezari, S., Giomi, M., Goldstein, D.A., Golkhou, V.Z., Goobar, A., Groom, S., Hacopians, E., Hale, D., Henning, J., Ho, A.Y.Q., Hover, D., Howell, J., Hung, T., Huppenkothen, D., Imel, D., Ip, W.H., Ivezić, Ž., Jackson, E., Jones, L., Juric, M., Kasliwal, M.M., Kaspi, S., Kaye, S., Kelley, M.S.P., Kowalski, M., Kramer, E., Kupfer,

- T., Landry, W., Laher, R.R., Lee, C.D., Lin, H.W., Lin, Z.Y., Lunnan, R., Giomi, M., Mahabal, A., Mao, P., Miller, A.A., Monkewitz, S., Murphy, P., Ngeow, C.C., Nordin, J., Nugent, P., Ofek, E., Patterson, M.T., Penprase, B., Porter, M., Rauch, L., Rebbapragada, U., Reiley, D., Rigault, M., Rodriguez, H., van Roestel, J., Rusholme, B., van Santen, J., Schulze, S., Shupe, D.L., Singer, L.P., Soumagnac, M.T., Stein, R., Surace, J., Sollerman, J., Szkody, P., Taddia, F., Terek, S., Van Sistine, A., van Velzen, S., Vestrand, W.T., Walters, R., Ward, C., Ye, Q.Z., Yu, P.C., Yan, L., Zolkower, J., 2019. The Zwicky Transient Facility: System Overview, Performance, and First Results. *PASP* 131, 018002. doi:10.1088/1538-3873/aaecbe, arXiv:1902.01932.
- Bellm, E.C., Kulkarni, S.R., Graham, M.J., Dekany, R., Smith, R.M., Riddle, R., Masci, F.J., Helou, G., Prince, T.A., Adams, S.M., Barbarino, C., Barlow, T., Bauer, J., Beck, R., Belicki, J., Biswas, R., Blagorodnova, N., Bodewits, D., Bolin, B., Brinnel, V., Brooke, T., Bue, B., Bulla, M., Burruss, R., Cenko, S.B., Chang, C.K., Connolly, A., Coughlin, M., Cromer, J., Cunningham, V., De, K., Delacroix, A., Desai, V., Duev, D.A., Eadie, G., Farnham, T.L., Feeney, M., Feindt, U., Flynn, D., Franckowiak, A., Frederick, S., Fremling, C., Gal-Yam, A., Gezari, S., Giomi, M., Goldstein, D.A., Golkhou, V.Z., Goobar, A., Groom, S., Hacıoğlu, E., Hale, D., Henning, J., Ho, A.Y.Q., Hover, D., Howell, J., Hung, T., Huppenkothen, D., Imel, D., Ip, W.H., Ivezić, Z., Jackson, E., Jones, L., Juric, M., Kasliwal, M.M., Kaspi, S., Kaye, S., Kelley, M.S.P., Kowalski, M., Kramer, E., Kupfer, T., Landry, W., Laher, R.R., Lee, C.D., Lin, H.W., Lin, Z.Y., Lunnan, R., Giomi, M., Mahabal, A., Mao, P., Miller, A.A., Monkewitz, S., Murphy, P., Ngeow, C.C., Nordin, J., Nugent, P., Ofek, E., Patterson, M.T., Penprase, B., Porter, M., Rauch, L., Rebbapragada, U., Reiley, D., Rigault, M., Rodriguez, H., Roestel, J.v., Rusholme, B., Santen, J.v., Schulze, S., Shupe, D.L., Singer, L.P., Soumagnac, M.T., Stein, R., Surace, J., Sollerman, J., Szkody, P., Taddia, F., Terek, S., Van Sistine, A., van Velzen, S., Vestrand, W.T., Walters, R., Ward, C., Ye, Q.Z., Yu, P.C., Yan, L., Zolkower, J., 2018. The Zwicky transient facility: System overview, performance, and first results. *Publications of the Astronomical Society of the Pacific* 131, 018002. URL: <https://doi.org/10.1088/1538-3873/aaecbe>, doi:10.1088/1538-3873/aaecbe.
- Betoule, M., Kessler, R., Guy, J., Mosser, J., Hardin, D., Biswas, R., Astier, P., El-Hage, P., Konig, M., Kuhlmann, S., Marnier, J., Pain, R., Regnault, N., Balland, C., Bassett, B.A., Brown, P.J., Campbell, H., Carlberg, R.G., Cellier-Holzem, F., Cinabro, D., Conley, A., D'Andrea, C.B., DePoy, D.L., Doi, M., Ellis, R.S., Fabbro, S., Filippenko, A.V., Foley, R.J., Frieman, J.A., Fouchez, D., Galbany, L., Goobar, A., Gupta, R.R., Hill, G.J., Hlozek, R., Hogan, C.J., Hook, I.M., Howell, D.A., Jha, S.W., Le Guillou, L., Leloudas, G., Lidman, C., Marshall, J.L., Möller, A., Mourão, A.M., Neveu, J., Nichol, R., Olmstead, M.D., Palanque-DeLabrouille, N., Perlmutter, S., Prieto, J.L., Pritchett, C.J., Richmond, M., Riess, A.G., Rühlmann-Kleider, V., Sako, M., Schahmanche, K., Schneider, D.P., Smith, M., Sollerman, J., Sullivan, M., Walton, N.A., Wheeler, C.J., 2014. Improved cosmological constraints from a joint analysis of the SDSS-II and SNLS supernova samples. *A&A* 568, A22. doi:10.1051/0004-6361/201423413, arXiv:1401.4064.
- Bloom, J.S., Richards, J.W., Nugent, P.E., Quimby, R.M., Kasliwal, M.M., Starr, D.L., Poznanski, D., Ofek, E.O., Cenko, S.B., Butler, N.R., Kulkarni, S.R., Gal-Yam, A., Law, N., 2012. Automating discovery and classification of transients and variable stars in the synoptic survey era. *Publications of the Astronomical Society of the Pacific* 124, 1175–1196. URL: <http://dx.doi.org/10.1086/668468>, doi:10.1086/668468.
- Breiman, L., 2001. Random forests. *Machine Learning* 45, 5–32. URL: <https://doi.org/10.1023/A:1010933404324>, doi:10.1023/A:1010933404324.
- Duev, D.A., Mahabal, A., Masci, F.J., Graham, M.J., Rusholme, B., Walters, R., Karmarkar, I., Frederick, S., Kasliwal, M.M., Rebbapragada, U., Ward, C., 2019. Real-bogus classification for the Zwicky transient facility using deep learning. *Monthly Notices of the Royal Astronomical Society* 489, 3582–3590. URL: <http://dx.doi.org/10.1093/mnras/stz2357>, doi:10.1093/mnras/stz2357.
- Gall, C., Stritzinger, M.D., Ashall, C., Baron, E., Burns, C.R., Hoefflich, P., Hsiao, E.Y., Mazzali, P.A., Phillips, M.M., Filippenko, A.V., Anderson, J.P., Benetti, S., Brown, P.J., Campillay, A., Challis, P., Contreras, C., Elias de la Rosa, N., Folatelli, G., Foley, R.J., Fraser, M., Holmbo, S., Marion, G.H., Morrell, N., Pan, Y.C., Pignata, G., Suntzeff, N.B., Taddia, F., Torres Robledo, S., Valenti, S., 2018. Two transitional type Ia supernovae located in the Fornax cluster member NGC 1404: SN 2007on and SN 2011iv. *A&A* 611, A58. doi:10.1051/0004-6361/201730886, arXiv:1707.03823.
- Gómez, P., Ruhberg, L.E., Nardone, M.T., O’Ryan, D., 2025. AnomalyMatch: Discovering Rare Objects of Interest with Semi-supervised and Active Learning. arXiv e-prints, arXiv:2505.03509doi:10.48550/arXiv.2505.03509, arXiv:2505.03509.
- Graham, M.L., Fremling, C., Perley, D.A., Biswas, R., Phillips, C.A., Sollerman, J., Nugent, P.E., Nance, S., Dhawan, S., Nordin, J., Goobar, A., Miller, A., Neill, J.D., Hall, X.J., Hankins, M.J., Duev, D.A., Kasliwal, M.M., Rigault, M., Bellm, E.C., Hale, D., Mróz, P., Kulkarni, S.R., 2022. Supernova siblings and their parent galaxies in the Zwicky Transient Facility Bright Transient Survey. *MNRAS* 511, 241–254. doi:10.1093/mnras/stab3802, arXiv:2112.14819.
- Ishida, E. E. O., Kornilov, M. V., Malanchev, K. L., Pruzhinskaya, M. V., Volnova, A. A., Korolev, V. S., Mondon, F., Sreejith, S., Malancheva, A. A., Das, S., 2021. Active anomaly detection for time-domain discoveries. *A&A* 650, A195. URL: <https://doi.org/10.1051/0004-6361/202037709>, doi:10.1051/0004-6361/202037709.

- Karpov, S., Peloton, J., 2023. The rate of satellite glints in ZTF and LSST sky surveys. *Contributions of the Astronomical Observatory Skalnaté Pleso* 53, 69–80. doi:10.31577/caosp.2023.53.4.69, arXiv:2310.17322.
- Kornilov, M., Korolev, V., Malanchev, K., Lavrukhina, A., Russeil, E., Semenikhin, T., Gangler, E., Ishida, E., Pruzhinskaya, M., Volnova, A., Sreejith, S., 2025. Coniferest: A complete active anomaly detection framework. *Astronomy and Computing* 52, 100960. URL: <https://www.sciencedirect.com/science/article/pii/S2213133725000332>, doi:<https://doi.org/10.1016/j.ascom.2025.100960>.
- Liu, F.T., Ting, K.M., Zhou, Z.H., 2008. Isolation forest, in: 2008 Eighth IEEE International Conference on Data Mining, pp. 413–422. doi:10.1109/ICDM.2008.17.
- LSST Science Collaboration, Abell, P.A., Allison, J., Anderson, S.F., Andrew, J.R., Angel, J.R.P., Armus, L., Arnett, D., Asztalos, S.J., Axelrod, T.S., Bailey, S., Ballantyne, D.R., Bankert, J.R., Barkhouse, W.A., Barr, J.D., Barrientos, L.F., Barth, A.J., Bartlett, J.G., Becker, A.C., Becla, J., Beers, T.C., Bernstein, J.P., Biswas, R., Blanton, M.R., Bloom, J.S., Bochanski, J.J., Boeshaar, P., Borne, K.D., Bradac, M., Brandt, W.N., Bridge, C.R., Brown, M.E., Brunner, R.J., Bullock, J.S., Burgasser, A.J., Burge, J.H., Burke, D.L., Cargile, P.A., Chandrasekharan, S., Chartas, G., Chesley, S.R., Chu, Y.H., Cinabro, D., Claire, M.W., Claver, C.F., Clowe, D., Connolly, A.J., Cook, K.H., Cooke, J., Cooray, A., Covey, K.R., Culliton, C.S., de Jong, R., de Vries, W.H., Debattista, V.P., Delgado, F., Dell’Antonio, I.P., Dhital, S., Di Stefano, R., Dickinson, M., Dilday, B., Djorgovski, S.G., Dobler, G., Donalek, C., Dubois-Felsmann, G., Durech, J., Eliasdottir, A., Eracleous, M., Eyer, L., Falco, E.E., Fan, X., Fassnacht, C.D., Ferguson, H.C., Fernandez, Y.R., Fields, B.D., Finkbeiner, D., Figueroa, E.E., Fox, D.B., Francke, H., Frank, J.S., Frieman, J., Fromenteau, S., Furqan, M., Galaz, G., Gal-Yam, A., Garnavich, P., Gawiser, E., Geary, J., Gee, P., Gibson, R.R., Gilmore, K., Grace, E.A., Green, R.F., Gressler, W.J., Grillmair, C.J., Habib, S., Haggerty, J.S., Hamuy, M., Harris, A.W., Hawley, S.L., Heavens, A.F., Hebb, L., Henry, T.J., Hileman, E., Hilton, E.J., Hoadley, K., Holberg, J.B., Holman, M.J., Howell, S.B., Infante, L., Ivezić, Z., Jacoby, S.H., Jain, B., Jedicke, J., Jee, M.J., Garrett Jernigan, J., Jha, S.W., Johnston, K.V., Jones, R.L., Juric, M., Kaasalainen, M., Styliani, Kafka, Kahn, S.M., Kaib, N.A., Kalirai, J., Kantor, J., Kasliwal, M.M., Keaton, C.R., Kessler, R., Knezevic, Z., Kowalski, A., Krabbendam, V.L., Krughoff, K.S., Kulkarni, S., Kuhlman, S., Lacy, M., Lepine, S., Liang, M., Lien, A., Lira, P., Long, K.S., Lorenz, S., Lotz, J.M., Lupton, R.H., Lutz, J., Macri, L.M., Mahabal, A.A., Mandelbaum, R., Marshall, P., May, M., McGehee, P.M., Meadows, B.T., Meert, A., Milani, A., Miller, C.J., Miller, M., Mills, D., Minniti, D., Monet, D., Mukadam, A.S., Nakar, E., Neill, D.R., Newman, J.A., Nikolaev, S., Nordby, M., O’Connor, P., Oguri, M., Oliver, J., Olivier, S.S., Olsen, J.K., Olsen, K., Olszewski, E.W., Oluseyi, H., Padilla, N.D., Parker, A., Pepper, J., Peterson, J.R., Petry, C., Pinto, P.A., Pizagno, J.L., Popescu, B., Prsa, A., Radcka, V., Raddick, M.J., Rasmussen, A., Rau, A., Rho, J., Rhoads, J.E., Richards, G.T., Ridgway, S.T., Robertson, B.E., Roskar, R., Saha, A., Sarajedini, A., Scannapieco, E., Schalk, T., Schindler, R., Schmidt, S., Schneider, D.P., Schumacher, G., Scranton, R., Seabag, J., Seppala, L.G., Shemmer, O., Simon, J.D., Sivertz, M., Smith, H.A., Allyn Smith, J., Smith, N., Spitz, A.H., Stanford, A., Stassun, K.G., Strader, J., Strauss, M.A., Stubbs, C.W., Sweeney, D.W., Szalay, A., Szkody, P., Takada, M., Thorman, P., Trilling, D.E., Trimble, V., Tyson, A., Van Berg, R., Vanden Berk, D., VanderPlas, J., Verde, L., Vrsnak, B., Walkowicz, L.M., Wandelt, B.D., Wang, S., Wang, Y., Warner, M., Wechsler, R.H., West, A.A., Wiecha, O., Williams, B.F., Willman, B., Wittman, D., Wolff, S.C., Wood-Vasey, W.M., Wozniak, P., Young, P., Zentner, A., Zhan, H., 2009. LSST Science Book, Version 2.0. doi:10.48550/arXiv.0912.0201, arXiv:0912.0201.
- Mahabal, A., Rebbapragada, U., Walters, R., Masci, F.J., Blagorodnova, N., Roestel, J.v., Ye, Q.Z., Biswas, R., Burdge, K., Chang, C.K., Duev, D.A., Golkhou, V.Z., Miller, A.A., Nordin, J., Ward, C., Adams, S., Bellm, E.C., Branton, D., Bue, B., Cannella, C., Connolly, A., Dekany, R., Feindt, U., Hung, T., Fortson, L., Frederick, S., Fremling, C., Gezari, S., Graham, M., Groom, S., Kasliwal, M.M., Kulkarni, S., Kupfer, T., Lin, H.W., Lintott, C., Lunnan, R., Parejko, J., Prince, T.A., Riddle, R., Rusholme, B., Saunders, N., Sedaghat, N., Shupe, D.L., Singer, L.P., Soumagnac, M.T., Szkody, P., Tachibana, Y., Tirumala, K., Velzen, S.v., Wright, D., 2019. Machine learning for the Zwicky transient facility. *Publications of the Astronomical Society of the Pacific* 131, 038002. URL: <https://doi.org/10.1088/1538-3873/aaf3fa>, doi:10.1088/1538-3873/aaf3fa.
- Majumder, T., Pruzhinskaya, M.V., Ishida, E.E.O., Malanchev, K.L., Semenikhin, T.A., 2024. Superluminous supernova search with pineforest. URL: <https://arxiv.org/abs/2410.21077>, arXiv:2410.21077.
- Malanchev, K., Kornilov, M.V., Pruzhinskaya, M.V., Ishida, E.E.O., Aleo, P.D., Korolev, V.S., Lavrukhina, A., Russeil, E., Sreejith, S., Volnova, A.A., Voloshina, A., Krone-Martins, A., 2023. The SNAD Viewer: Everything You Want to Know about Your Favorite ZTF Object. *PASP* 135, 024503. doi:10.1088/1538-3873/acb292, arXiv:2211.07605.
- Malanchev, K.L., Pruzhinskaya, M.V., Korolev, V.S., Aleo, P.D., Kornilov, M.V., Ishida, E.E.O., Krushinsky, V.V., Mondon, F., Sreejith, S., Volnova, A.A., Belinski, A.A., Dodin, A.V., Tatarnikov, A.M., Zheltoukhov, S.G., (The SNAD Team), 2021. Anomaly detection in the Zwicky Transient Facility DR3. *MNRAS* 502, 5147–5175. doi:10.1093/mnras/stab316, arXiv:2012.01419.
- Masci, F.J., Laher, R.R., Rusholme, B., Shupe, D.L., Groom, S., Surace, J., Jackson, E., Monkewitz, S., Beck, R., Flynn,

- D., Terek, S., Landry, W., Hacopians, E., Desai, V., Howell, J., Brooke, T., Imel, D., Wachter, S., Ye, Q.Z., Lin, H.W., Cenko, S.B., Cunningham, V., Rebbapragada, U., Bue, B., Miller, A.A., Mahabal, A., Bellm, E.C., Patterson, M.T., Juric, M., Golkhou, V.Z., Ofek, E.O., Walters, R., Graham, M., Kasliwal, M.M., Dekany, R.G., Kupfer, T., Burdge, K., Cannella, C.B., Barlow, T., Van Sistine, A., Giomi, M., Fremling, C., Blagorodnova, N., Levitan, D., Riddle, R., Smith, R.M., Helou, G., Prince, T.A., Kulkarni, S.R., 2019. The Zwicky Transient Facility: Data Processing, Products, and Archive. *PASP* 131, 018003. doi:10.1088/1538-3873/aae8ac, arXiv:1902.01872.
- Perley, D.A., Fremling, C., Sollerman, J., Miller, A.A., Dahi-wale, A.S., Sharma, Y., Bellm, E.C., Biswas, R., Brink, T.G., Bruch, R.J., De, K., Dekany, R., Drake, A.J., Duev, D.A., Filippenko, A.V., Gal-Yam, A., Goobar, A., Graham, M.J., Graham, M.L., Ho, A.Y.Q., Irani, I., Kasliwal, M.M., Kim, Y.L., Kulkarni, S.R., Mahabal, A., Masci, F.J., Modak, S., Neill, J.D., Nordin, J., Riddle, R.L., Soumagnac, M.T., Strotjohann, N.L., Schulze, S., Taggart, K., Tzanidakis, A., Walters, R.S., Yan, L., 2020. The zwicky transient facility bright transient survey. ii. a public statistical sample for exploring supernova demographics*. *The Astrophysical Journal* 904, 35. URL: <http://dx.doi.org/10.3847/1538-4357/abbd98>, doi:10.3847/1538-4357/abbd98.
- Potantin, S.A., Belinski, A.A., Dodin, A.V., Zheltoukhov, S.G., Lander, V.Y., Postnov, K.A., Savvin, A.D., Tatarnikov, A.M., Cherepashchuk, A.M., Cheryasov, D.V., Chilingarian, I.V., Shatsky, N.I., 2020. Transient Double-Beam Spectrograph for the 2.5-m Telescope of the Caucasus Mountain Observatory of SAI MSU. *Astronomy Letters* 46, 836–854. doi:10.1134/S1063773720120038, arXiv:2011.03061.
- Pruzhinskaya, M.V., Malanchev, K.L., Kornilov, M.V., Ishida, E.E.O., Mondon, F., Volnova, A.A., Korolev, V.S., 2019. Anomaly detection in the Open Supernova Catalog. *MNRAS* 489, 3591–3608. doi:10.1093/mnras/stz2362, arXiv:1905.11516.
- Pruzhinskaya, M. V., Ishida, E. E. O., Novinskaya, A. K., Russeil, E., Volnova, A. A., Malanchev, K. L., Kornilov, M. V., Aleo, P. D., Korolev, V. S., Krushinsky, V. V., Sreejith, S., Gangler, E., 2023. Supernova search with active learning in ztf dr3. *A&A* 672, A111. URL: <https://doi.org/10.1051/0004-6361/202245172>, doi:10.1051/0004-6361/202245172.
- Richards, J.W., Starr, D.L., Butler, N.R., Bloom, J.S., Brewer, J.M., Crellin-Quick, A., Higgins, J., Kennedy, R., Rischard, M., 2011. On machine-learned classification of variable stars with sparse and noisy time-series data. *The Astrophysical Journal* 733, 10. URL: <https://doi.org/10.1088/0004-637X/733/1/10>, doi:10.1088/0004-637X/733/1/10.
- Salo, L., Zhou, R., Johnson, S., Kelly, P., Jones, G.L., 2025. Supernova Siblings and Spectroscopic Host Galaxy Properties. *ApJ* 981, 97. doi:10.3847/1538-4357/adad60, arXiv:2504.04641.
- Schlafly, E.F., Finkbeiner, D.P., 2011. Measuring Reddening with Sloan Digital Sky Survey Stellar Spectra and Recalibrating SFD. *ApJ* 737, 103. doi:10.1088/0004-637X/737/2/103, arXiv:1012.4804.
- Semenikhin, T., 2025. SNAD Transient Discovery Report for 2025-07-30. Transient Name Server Discovery Report 2025-2992, 1.
- Semenikhin, T., Kornilov, M., Pruzhinskaya, M., Lavrukhina, A., Russeil, E., Gangler, E., Ishida, E., Korolev, V., Malanchev, K., Volnova, A., Sreejith, S., 2025. Real-bogus scores for active anomaly detection. *Astronomy and Computing* 51, 100919. URL: <https://www.sciencedirect.com/science/article/pii/S2213133724001343>, doi:<https://doi.org/10.1016/j.ascom.2024.100919>.
- Shatsky, N., Belinski, A., Dodin, A., Zheltoukhov, S., Kornilov, V., Postnov, K., Potanin, S., Safonov, B., Tatarnikov, A., Cherepashchuk, A., 2020. The Caucasian Mountain Observatory of the Sternberg Astronomical Institute: First Six Years of Operation, in: Romanuk, I.I., Yakunin, I.A., Valeev, A.F., Kudryavtsev, D.O. (Eds.), *Ground-Based Astronomy in Russia. 21st Century*, pp. 127–132. doi:10.26119/978-5-6045062-0-2_2020_127, arXiv:2010.10850.
- Smith, N., Li, W., Silverman, J.M., Ganeshalingam, M., Filippenko, A.V., 2011. Luminous blue variable eruptions and related transients: diversity of progenitors and outburst properties. *MNRAS* 415, 773–810. doi:10.1111/j.1365-2966.2011.18763.x, arXiv:1010.3718.
- Stein, R., Callis, E., Kostrzewa-Rutkowska, Z., Fraser, M., Yaron, O., 2018. ePESSTO Transient Classification Report for 2018-08-13. Transient Name Server Classification Report 2018-2128, 1.
- Tonry, J., Denneau, L., Weiland, H., Lawrence, A., Siverd, R., Erasmus, N., Koorts, W., Anderson, J., Jordan, A., Suc, V., Smartt, S.J., Smith, K.W., Srivastav, S., Young, D.R., Nicholl, M., Fulton, M., McCollum, M., Moore, T., Weston, J., Sheng, X., Aamer, A., Shingles, L., Rest, A., Chen, T.W., Stubbs, C., Sommer, J., Rhodes, L., Andersson, A., 2023. ATLAS Transient Discovery Report for 2023-06-16. Transient Name Server Discovery Report 2023-1398, 1.
- Tonry, J., Stalder, B., Denneau, L., Heinze, A., Weiland, H., Rest, A., Smith, K.W., Smartt, S.J., Young, D.R., Fulton, M., McBrien, O., O'Neill, D., Clark, P., 2018. ATLAS Transient Discovery Report for 2018-07-30. Transient Name Server Discovery Report 2018-1055, 1.
- Villar, V.A., Cranmer, M., Berger, E., Contardo, G., Ho, S., Hosseinzadeh, G., Lin, J.Y.Y., 2021. A deep-learning

approach for live anomaly detection of extragalactic transients. *The Astrophysical Journal Supplement Series* 255, 24. URL: <https://doi.org/10.3847/1538-4365/ac0893>, doi:10.3847/1538-4365/ac0893.

Webb, S., Lochner, M., Muthukrishna, D., Cooke, J., Flynn, C., Mahabal, A., Goode, S., Andreoni, I., Pritchard, T., Abbott, T.M.C., 2020. Unsupervised machine learning for transient discovery in deeper, wider, faster light curves. *Monthly Notices of the Royal Astronomical Society* 498, 3077–3094. URL: <https://doi.org/10.1093/mnras/staa2395>, doi:10.1093/mnras/staa2395, arXiv:<https://academic.oup.com/mnras/article-pdf/498/3/3077/33780541/staa2395.pdf>.

Wright, D.E., Smartt, S.J., Smith, K.W., Miller, P., Kotak, R., Rest, A., Burgett, W.S., Chambers, K.C., Flewelling, H., Hodapp, K.W., Huber, M., Jedicke, R., Kaiser, N., Metcalfe, N., Price, P.A., Tonry, J.L., Wainscoat, R.J., Waters, C., 2015. Machine learning for transient discovery in pan-starrs1 difference imaging. *Monthly Notices of the Royal Astronomical Society* 449, 451–466. URL: <https://doi.org/10.1093/mnras/stv292>, doi:10.1093/mnras/stv292, arXiv:<https://academic.oup.com/mnras/article-pdf/449/1/451/4139177/stv292.pdf>.

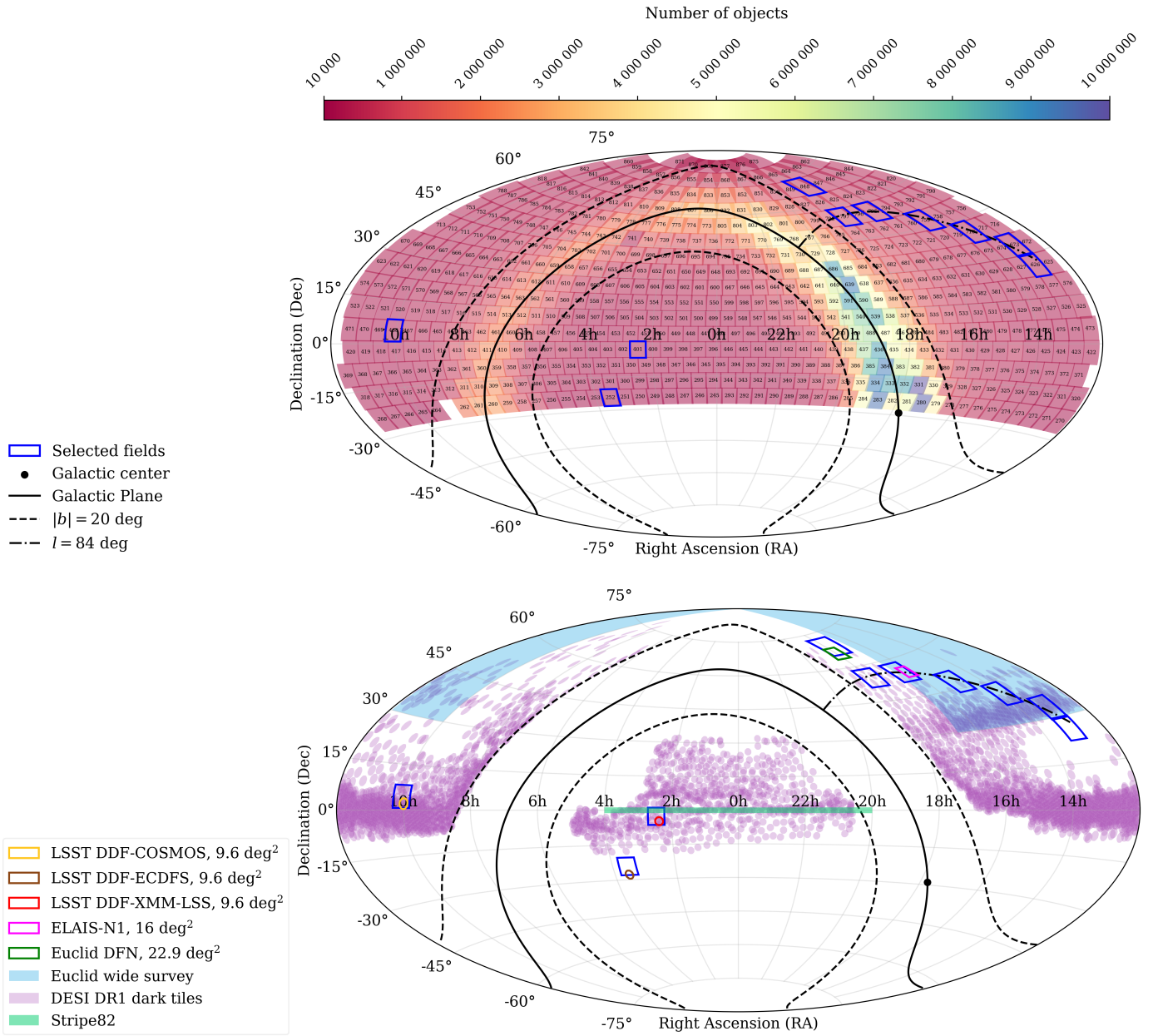


Figure 1: Sky maps illustrating the selection of ZTF fields used in this study. **Top:** Distribution of object counts from the main dataset across ZTF fields (numbers within rectangles indicate the corresponding Field ID); blue rectangles mark the ten selected fields. **Bottom:** The same ten ZTF fields shown in relation to the sky coverage of other big surveys.

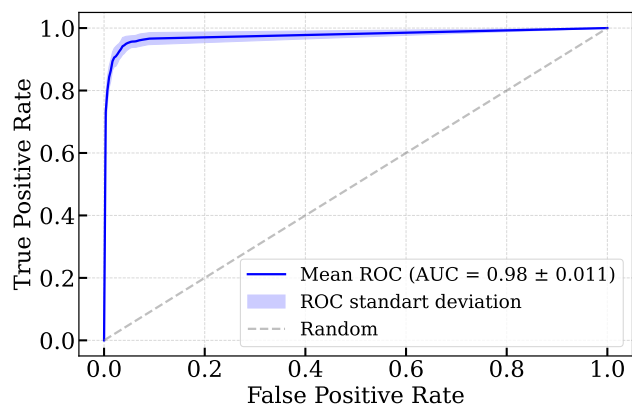


Figure 2: Mean ROC curve across stratified k-fold validation folds, with the shaded band indicating $\pm\sigma$ variability.

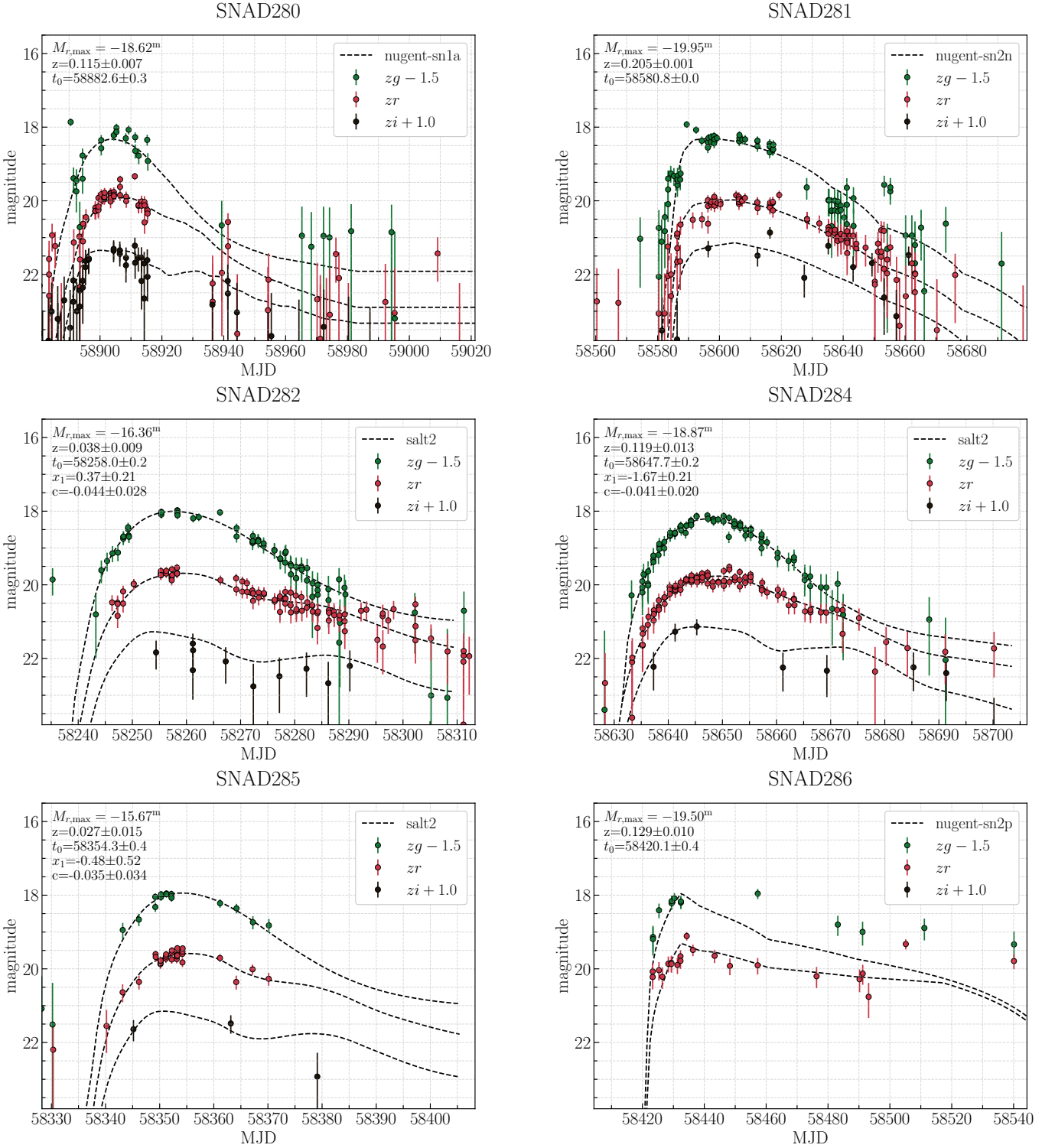


Figure 3: ZTF DR23 multicolor light curves of new supernova candidates with SNCOSMO best-model fits and fitted model parameters.

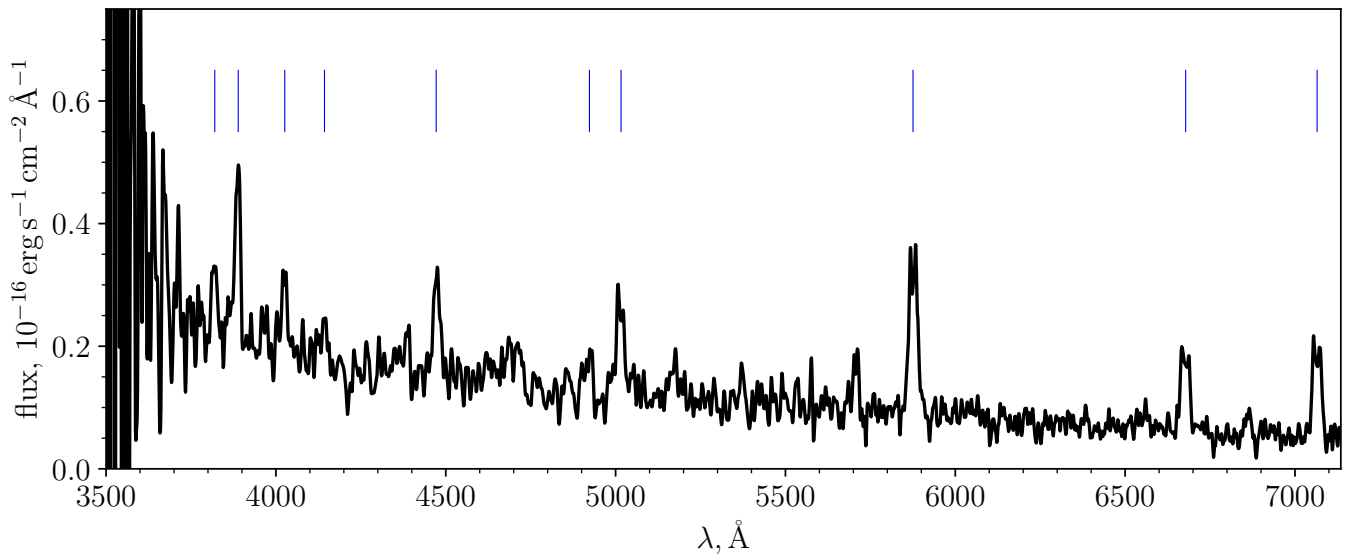


Figure 4: The spectrum of SNAD283 obtained with the 2.5-meter telescope of the Caucasus Mountain Observatory. Blue markers indicate the positions of HeI double-peaked emission lines.

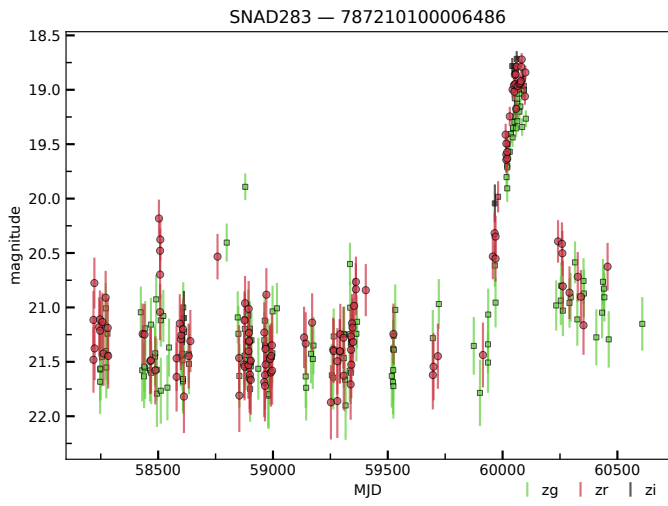


Figure 5: ZTF DR23 multicolor light curve of SNAD283 generated with the SNAD ZTF Viewer (Malanchev et al., 2023).

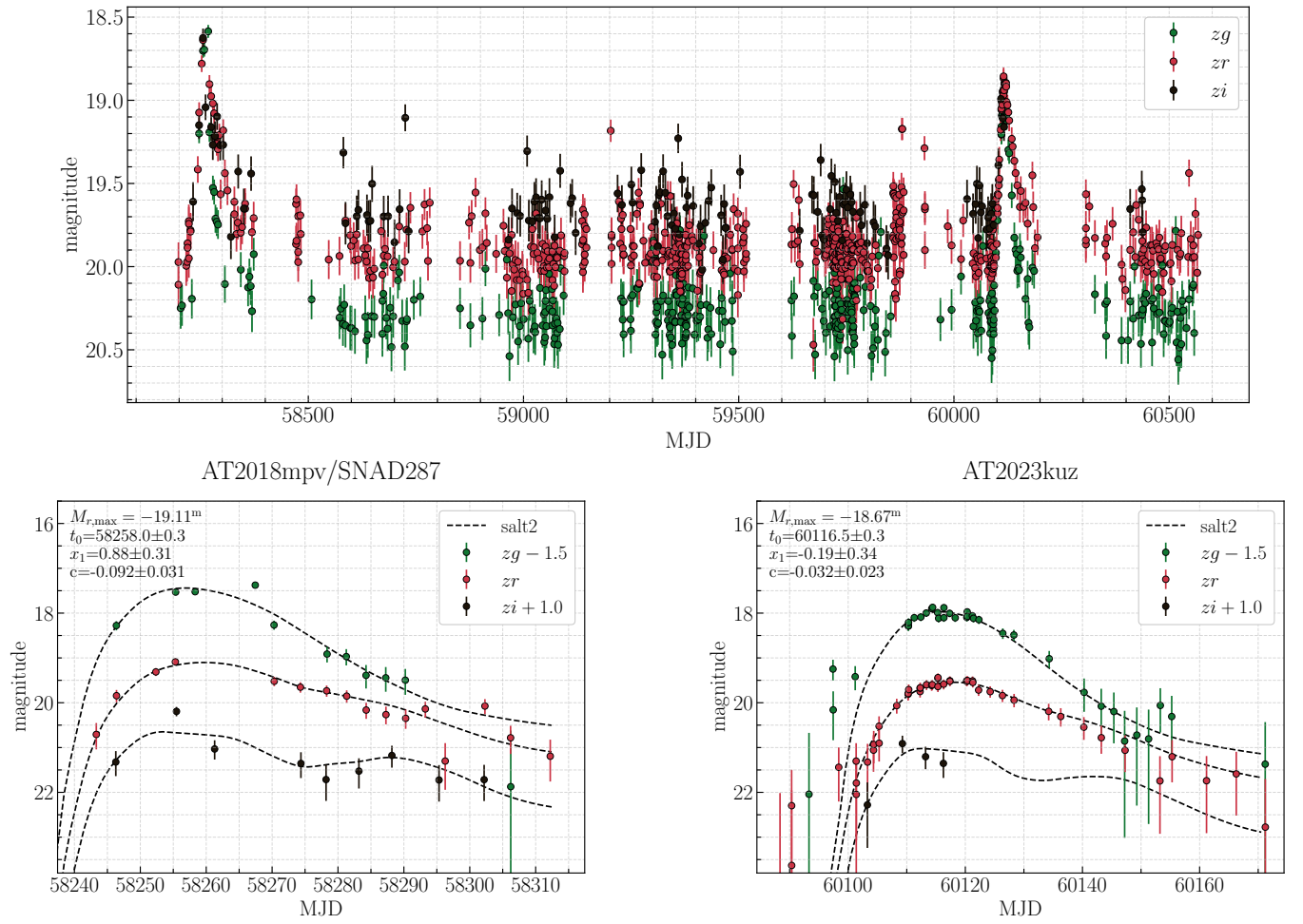


Figure 6: Top: ZTF DR23 light curves of the multiple supernovae AT2018mpv/SNAD287 and AT2023kuz/ATLAS23mmv. Bottom: separate SMCOSMO fits to the light curves of both outbursts, with the corresponding best-fit model parameters.

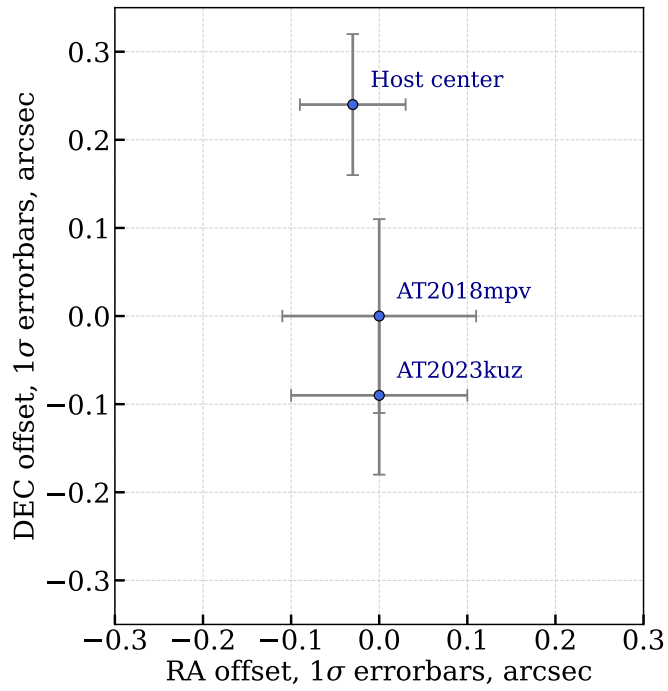


Figure 7: Relative offsets between the two outbursts, AT2018mpv/SNAD287 and AT2023kuz/ATLAS23mmv, and the host galaxy center. The sources positions were measured from stacked ZTF zr -band images using two-dimensional Gaussian fitting.

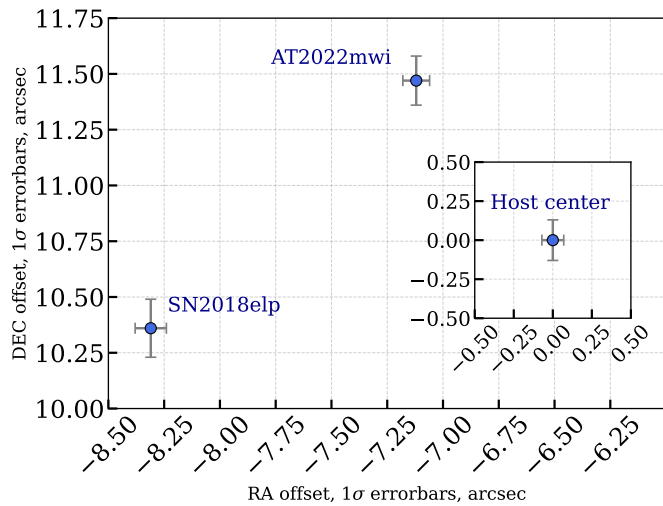


Figure 8: Relative offsets between the two outbursts, SN2018elp and AT2022mwi, and the host galaxy center. The sources positions were measured from stacked ZTF zr -band images using two-dimensional Gaussian fitting.

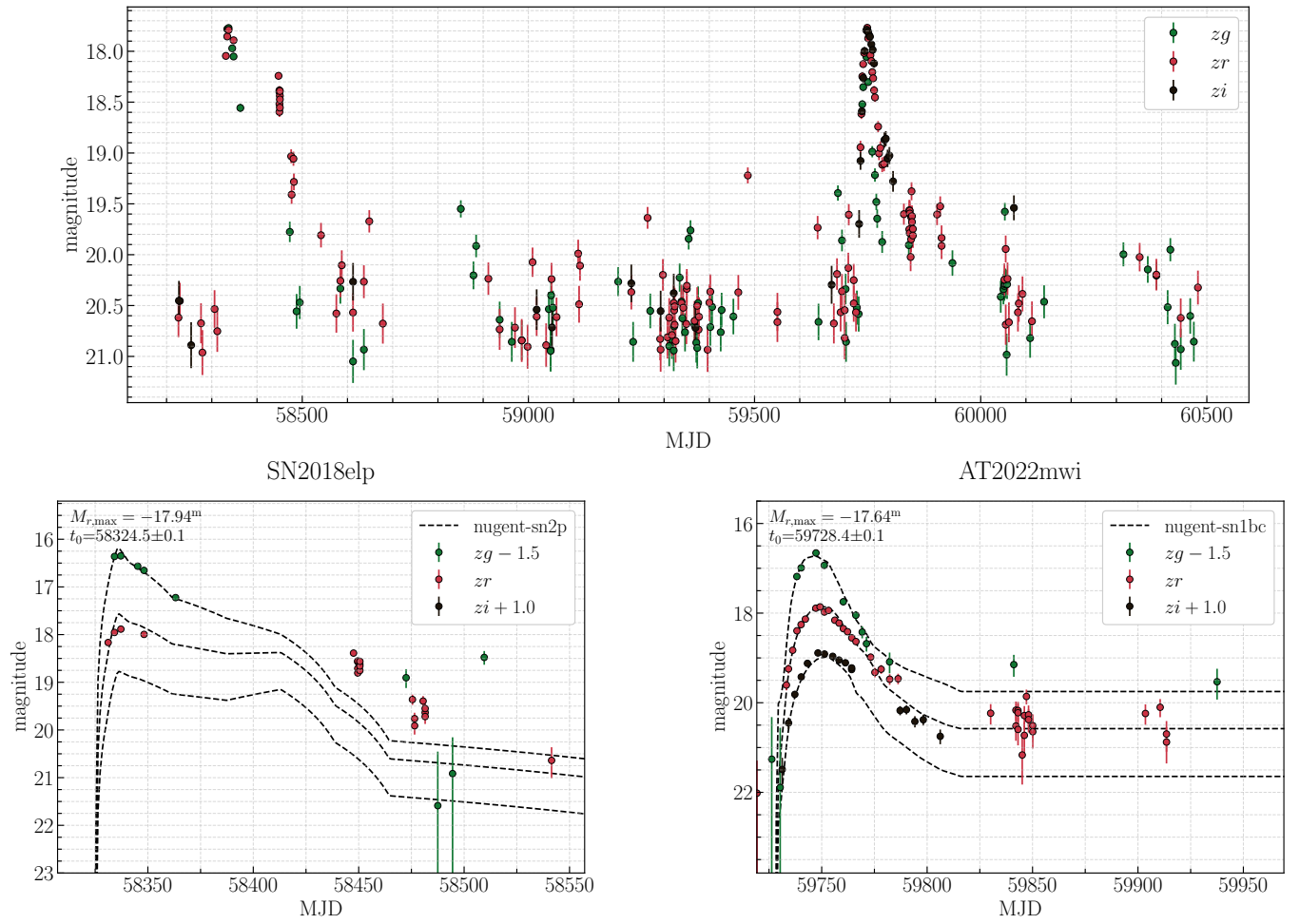


Figure 9: Top: ZTF DR23 light curves of the multiple supernovae SN2018elp and AT2022mwi. Bottom: separate SMCOSMO fits to the light curves of both outbursts, with the corresponding best-fit model parameters.